

## X-RAY LINE EMISSION IN HERCULES X-1

M.A. Jimenez-Garate<sup>1</sup>, C.J. Hailey<sup>2</sup>, J.W. den Herder<sup>3</sup>, S. Zane<sup>4</sup>, and G. Ramsay<sup>4</sup>

<sup>1</sup>MIT Center for Space Research, 77 Vassar St. Room 37-274, NE80-6091, Cambridge, MA, 02139, USA

<sup>2</sup>Columbia Astrophysics Laboratory, 550 West 120th St, New York, NY, 10027, USA

<sup>3</sup>Space Research Organization of The Netherlands, Sorbonnelaan 2, 3584 CA Utrecht, The Netherlands

<sup>4</sup>Mullard Space Science Laboratory, University College London, Holmbury St. Mary, Dorking, Surrey, RH5 6NT, England, UK

### ABSTRACT

We find line emission from the hydrogen- and/or helium-like ions of Ne, O, N and C in the low and short-on states of Her X-1, using the *XMM-Newton* Reflection Grating Spectrometer. The emission line velocity broadening is  $200 < \sigma < 500 \text{ km s}^{-1}$ . Plasma diagnostics with the Ne IX, O VII and N VI He $\alpha$  lines and the radiative recombination continua of O VII and N VII, indicate the gas is heated by photoionization, with an electron temperature of  $T = 6 \pm 2 \text{ eV}$ . We use spectral models to measure element abundance ratios of  $[\text{N}/\text{O}] = 9.5 \pm 1.3$ ,  $[\text{C}/\text{O}] = 0.68 \pm 0.16$ , and  $[\text{Ne}/\text{O}] = 2.4 \pm 1.2$  times solar, which quantify CNO processing in HZ Her. Photoexcitation and high-density effects are not differentiated by the measured He $\alpha$  lines, as shown by calculations that use previous UV photometry. We set limits on the location of the line emission region, and find an electron density  $n_e > 10^{11} \text{ cm}^{-3}$ . The narrow emission lines can be attributed to reprocessing in either an accretion disk atmosphere and corona or on the X-ray illuminated face of HZ Her. In the main-on state, the bright continuum only allows the detection of interstellar absorption, plus O VII He $\alpha$  emission lines with  $\sigma = 3200 \pm 700 \text{ km s}^{-1}$  and complex profiles. Other broad lines may be present. The broad lines may originate in a region near the pulsar magnetosphere. In such a case, periodic occultations of the Her X-1 magnetosphere must occur with 35 d phase, consistent with the precession of the accretion disk. Fe L lines are not detected.

**Key words:** X-rays: binaries — line: formation — line: identification — pulsars: individual — accretion, accretion disks

### 1. INTRODUCTION

In Her X-1, X-rays are being generated by the infall of plasma from a  $2.3 M_\odot$  star (HZ Her) onto a  $1.5 \pm 0.3 M_\odot$  neutron star (Reynolds et al. 1997). The neutron star pulsates in the X-ray band with period  $P_{\text{pulse}} = 1.24$  (Tananbaum et al. 1972). The thermal emission observed in the soft X-ray band, the large luminosity of the system ( $L = 3.8 \times 10^{37} \text{ erg s}^{-1}$ ), and the observed broad UV emission lines (Boroson et al. 1997), all indicate the mass

transfer is being mediated by an accretion disk. Her X-1 is unusually well placed for soft X-ray and UV observations, since it is  $\sim 3$  kpc above the galactic plane while at a distance of  $6.6 \pm 0.4$  kpc (Reynolds et al. 1997). An orbital period of  $P_{\text{orb}} = 40^{h}8$  can be measured from X-ray eclipses (Tananbaum et al. 1972).

One of our main goals is to find the spectral signatures of a precessing accretion disk. The Her X-1 system goes through high and low X-ray flux states in an almost periodic fashion, with a  $P_\psi = 35 \text{ d}$  pseudo-period (Giacconi et al. 1973). Variability as a function of  $\psi$  has also been observed in the optical light curves (Gerend & Boynton 1976), X-ray pulse shapes (Deeter et al. 1991), X-ray dips (Scott & Leahy 1999), and X-ray spectra (Ramsay et al. 2002 and this paper). The  $\psi$ -phase has been associated with disk precession (Petterson et al. 1991; Scott et al. 2000). Only a handful of other X-ray sources are known to exhibit such pseudo-periodicities, and Her X-1 is the brightest of the group. The binary system is being observed nearly edge-on, at an inclination angle of  $i \sim 85^\circ$ . Models of the disk atmosphere and corona (Jimenez-Garate et al. 2001) show that its line emission is detectable, especially at large  $i$  and in binaries with large ( $\sim 10^{11} \text{ cm}$ ) disks. Her X-1 is also a prime object to study the interaction of an accretion disk with a strong magnetic field ( $B = 3.5 \times 10^{12} \text{ G}$  from dal Fiume et al. 1998, Truemper et al. 1978).

### 2. SPECTROSCOPY WITH RGS

Three observations with the *XMM-Newton* Reflection Grating Spectrometer (*RGS*), during the low, short-on and main-on states, reveal recombination line and continuum emission in Her X-1. We find dramatic spectral changes through the 35 d cycle, including changes in the continuum, line fluxes, and line widths. The high resolution X-ray spectra unveil two new components inside the Her X-1 system:

1. A photoionized narrow-line region, with velocity broadening  $\sim 300 \text{ km s}^{-1}$ . The density of this material is  $n_e > 10^{11} \text{ cm}^{-3}$ , with the lowest temperatures in the  $20,000 < T < 70,000 \text{ K}$  range. We set an upper bound for the radius of this region of  $r < 10^{12} \text{ cm}$ , just outside the  $3 \times 10^{11} \text{ cm}$  Roche lobe radius.
2. A photoionized broad-line region evidenced by O VII He $\alpha$  lines with velocity broadening  $\sim 3,500 \text{ km s}^{-1}$ . If

the broadening is due to orbital velocity, this region is between  $5 \times 10^8 < r < 3 \times 10^9$  cm. We estimate the density of this region to be  $10^{16} < n_e < 10^{19}$  cm $^{-3}$ .

### 2.1. LOW AND SHORT-ON STATES: NARROW LINE EMISSION

The low and short-on state spectra consist of a power-law continuum plus radiative recombination (*RR*) emission. The brightest line features have a velocity broadening  $200 < \sigma < 500$  km s $^{-1}$ . The count rate in the short-on is twice as that in the low state, for both continuum and most lines. The N VI, O VII, and Ne IX triplet ratios indicate the gas is photoionized (section 3). The power-law continuum is probably due to Compton scattering of the neutron star X-rays in the accretion disk corona and/or on the face of the companion.

The variation of the X-ray line flux with 35 d phase, vis-a-vis the expected accretion disk inclination from Scott et al. (2000), suggests that at least half of the line emission originates on the face of the companion. If the accretion disk atmosphere and corona are the only source of X-ray lines, then we expect the outer-disk inclination  $i_d$  to be in disagreement with the Scott et al. (2000) values. As the disk precesses from  $i_d \sim 90^\circ$  to  $i_d \sim 80^\circ$ , the observed lines should increase their flux and broadening, because the inner-disk becomes unobstructed by the outer-disk (Jimenez-Garate et al. 2001). According to the  $i_d(\psi)$  from Scott et al. (2000), the disk was more edge-on during the short-on than during the low state observation. If the line emission originates on the HZ Her, this can be explained by shadowing from the disk.

### 2.2. THE MAIN-ON: MAGNETOSPHERE EMISSION?

The main-on state in the 5–38 Å band is dominated by a smooth continuum and a broad continuum "bump" previously identified with Fe L line emission (see figure 2). Most of the soft X-ray continuum originates from reprocessing on the disk, judging by its sinusoidal pulse profile. The sharply peaked pulse profile observed below  $\sim 10$  Å (Ramsay et al. 2002), indicates the emission region is compact ( $< 10^8$  cm), and near the neutron star. The 10–15 Å "bump" does not contain any obvious Fe L lines. The continuum shape is complex and has not been successfully fitted yet with a model.

Weaker, discrete spectral features are present as well. A surprisingly broad O VII He $\alpha$  line complex, with  $\sigma = 3200^{+600}_{-700}$  km s $^{-1}$ , is centered on the *i* line, and is consistent with the line ratios observed in the low and short-on states. A weaker, similarly broad N VII Ly $\alpha$  line may also be present. High density plasma funneled out of the disk by the magnetic field forms a magnetospheric shell which may produce recombination emission as it is blasted by pulsar X-rays. If the magnetospheric ions are fully stripped of electrons, photons which are Compton scattered by those electrons may illuminate the neighboring

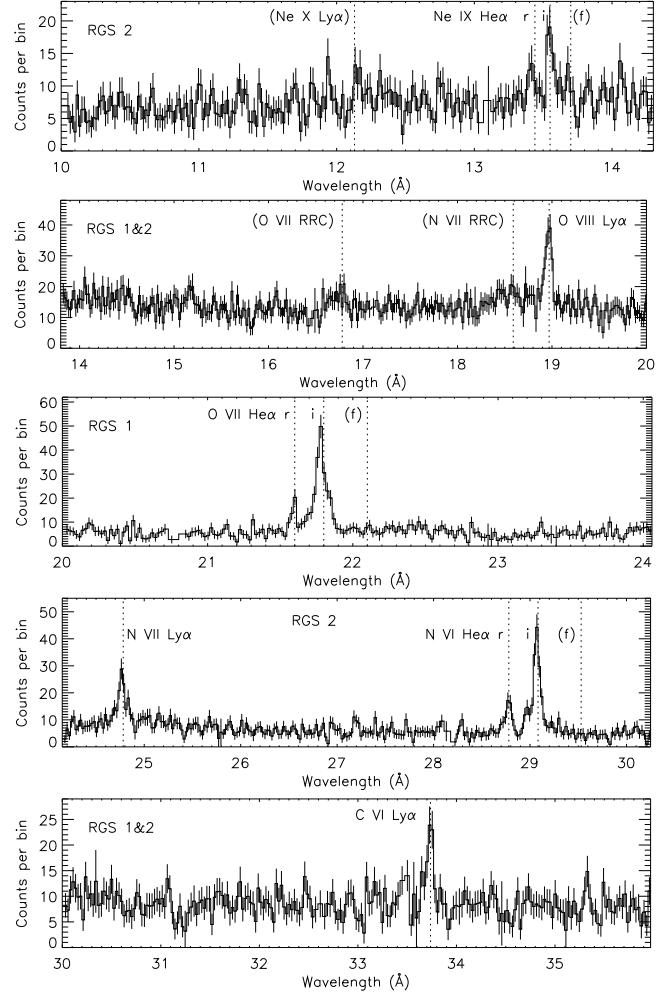


Figure 1. The added RGS spectrum of low and short-on state observations (of 12 and 13 ks). The bin size is 18, 21, 23, 25, and 27 mÅ for each successive frame, from short to long wavelengths.

disk and produce recombination (see figure 3). A 1s-2p resonant absorption feature from atomic O is detected. A neutral O edge is mostly instrumental in nature. The second order effective area also seems overestimated by the calibration below  $\sim 10$  Å, if we take the first order as reference. There is marginal evidence for a complex line shape, possibly a P Cygni with  $v > 2000$  km s $^{-1}$ , in O VIII Ly $\alpha$  (figure 2). P Cygni profiles for winds with velocities of  $v \sim 800$  km s $^{-1}$  have been found by Chiang (2001) in the UV. The upper bounds for the fluxes of unresolved lines are below those observed in the low and short-on states, for many of the lines (see figure 1). This may be due to an orbital phase ( $\phi$ ) dependence of the line fluxes, since the main-on observation was performed at  $\phi \simeq 0.22$ , while the other two observations were obtained at  $\phi \simeq 0.50$ , suggesting the narrow lines originate on HZ Her.

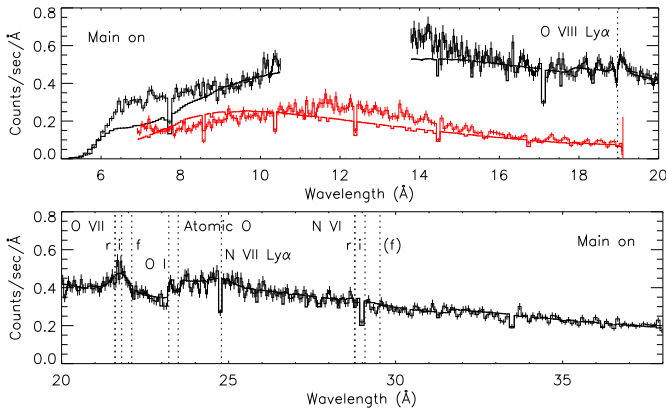


Figure 2. High-resolution spectrum with RGS 1 (histograms with error bars) in the main-on state observation at orbit 207 (11 ks). The power-law continuum model (thick-line histograms) is meant to emphasize the "bump" at 10–15 Å. Both first (black) and second order (red) spectra are shown.

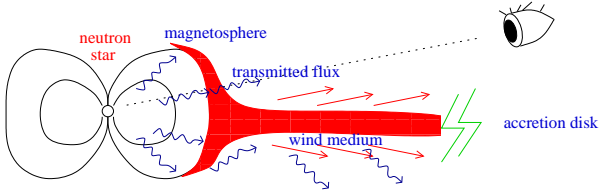


Figure 3. Sketch of the hypothetical inner region of the accretion disk and its interface with the magnetosphere. The broad line region coincides with the magnetosphere or the neighboring disk. The 1 keV "bump" could be an absorption complex from the photoionized gas at the base of the magnetosphere, which can be observed at high inclination. P Cygni profiles may form in the disk wind for optically thick lines (i.e. O VIII Ly $\alpha$ ). The disk is warped and its scale height increases with radius (not shown). The scale is  $\sim 10^9$  cm (neutron star radius  $\sim 10^6$  cm).

### 3. PLASMA DIAGNOSTICS

We use five kinds of spectral diagnostics:

1. The  $G$  ratio in He-like ion line triplets. The triplet consists of a resonance ( $r$ ), intercombination ( $i$ ) and a forbidden ( $f$ ) line. The plasma is found to be dominated by photoionization since the  $G = (i+f)/r \simeq 4.2$ . In contrast, collisional plasmas have  $G \sim 1$  (Liedahl 1999).
2. The  $R = f/i$  line ratio as density diagnostic in He-like ions. When the density is higher than some threshold,  $R \rightarrow 0$ , while in the low density limit,  $R \sim 4$  (Porquet & Dubau 2000). We observe  $R < 0.1$ .
3. The  $R$  ratio as UV radiation probe in He-like ions. Excitation by UV photons can also explain  $R \rightarrow 0$  (Mewe & Schrijver 1978, Kahn et al. 2001). We find photoexcitation competes with electron impact excitation. Using UV photometry from Boroson et al. (1997), we set  $r < 10^{12}$  cm for the radius of the line emission region.
4. Temperature diagnostics with the radiative recombination continuum ( $RRC$ ) (Liedahl & Paerels 1996). The width of the  $RRC$  is proportional to the electron temperature. For O VII and N VII, we find  $kT = 4 \pm 2$  eV and  $kT = 6 \pm 2$  eV, respectively. Model calculations with *XSTAR* v.2.1d (Kallman & McCray 1982) show  $2 < T < 4$  eV for N VII and O VII.
5. Using the ionization parameter, and assuming thermal and ionization balance in the optically thin case, we constrain the density to  $n_e > 4 \times 10^{11}$  cm $^{-3}$  for the narrow line region, and  $4 \times 10^{16} < n_e < 10^{19}$  cm $^{-3}$  for the broad line region of the main-on state. We use the limits on the distance to the pulsar that we set from photoexcitation and from velocity broadening.

### 4. EMISSION MEASURE ANALYSIS

This analysis allows us to measure or set limits on the density, geometry, and element abundances of the emission regions. We use plasma and spectral models together with a phenomenological emission measure distribution to fit the observed line fluxes. The emission measure,  $EM = \int n_e^2 dV$ , equals the volume times the density squared. The  $EM$  is proportional to the recombination line flux. The  $EM$  may vary as a function of the ionization parameter  $\xi = L/n_e r^2$ . To fit the line fluxes, we need the differential emission measure  $DEM = d(EM)/d(\log_{10} \xi)$  (as defined in Liedahl 1999). We use recombination rates calculated by Liedahl (private communication) with the *HULLAC* atomic code (Klapisch et al. 1977).

In one model, the emission measure is constant with respect to  $\xi$ , while in a second model, we let the  $DEM$  vary as a power law of  $\xi$ . The results of model 1, shown in figure 4, show that element abundance ratios differ from the solar values. The  $DEM$  of N and O is seen to depend on the charge state, invalidating model 1. The line flux variability, however, is well-represented by figure 4. Unlike the flat- $DEM$  model 1, the power-law  $DEM$  model 2 achieves self-consistency, and from it, element abundance ratios are extracted. We find  $[C/O] = 0.68 \pm 0.16$ ,  $[N/O] = 9.9 \pm 1.3$  and  $[Ne/O] = 2.4 \pm 1.0$  times solar for the low state data, using the solar abundances from Wilms et al. (2000). Nitrogen is significantly enriched, indicating CNO processing in HZ Her. A lower limit of  $n_e > 10^{14}$  cm $^{-3}$  is estimated from model 1 for the broad line region, by using the maximum volume deduced from velocity broadening.

### 5. CONCLUSIONS

The X-ray emission lines from Her X-1 are weak, but they provide a wealth of information on gas which is too hot to observe at other wavelengths and which may be very close to the neutron star. By use of models, the X-ray spectrum yields more accurate element abundance ratios between

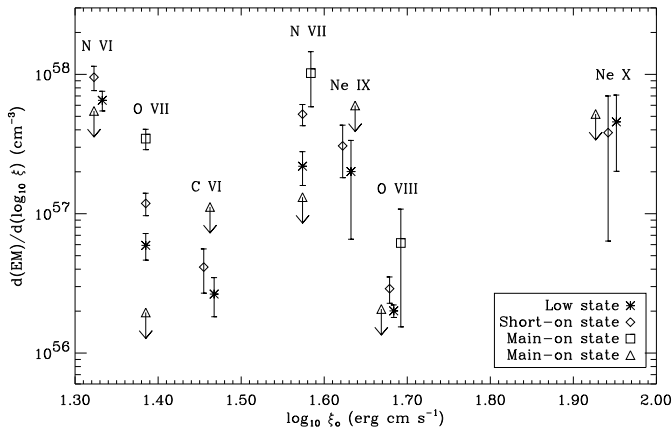


Figure 4. The differential emission measure (DEM) for the line emission detected at various Her X-1 states, versus the ionization parameter which maximizes the line power. We create a model with a flat DEM from  $0.0 < \log_{10} \xi < 3.5$ . Upper limits for the DEMs of unresolved lines in the main-on are denoted by triangles.

C, N, O, and Ne, constraining the historical nuclear burning in HZ Her. The temperature can be measured, and limits on the density and geometry of the gas are set. Two dynamically distinct photoionized regions are identified. A low dispersion velocity region may be the accretion disk atmosphere and corona, or the illuminated face of HZ Her. The high dispersion velocity region, albeit weakly detected, may be dense material in the magnetosphere or its neighboring inner-disk.

The high resolution X-ray spectrum of Her X-1 varies dramatically with 35 d phase, presumably due to the precession of the accretion disk. This spectral variability may help us determine the inclination-dependence of spectra from other X-ray binaries with disks.

Many features known to be present in the spectrum of photoionized gases have not been detected due to the low signal-to-noise of these data. In particular, the Lyman series lines provide constraints on the column density and line optical depth, and accurate measurements of the *RRC* verify the validity of the plasma equilibrium calculations used here. This will allow us to identify the source of the line emission and further investigate the environment around accreting neutron stars.

## REFERENCES

Boroson, B., Blair, W. P., Davidsen, A. F., Vrtilek, S. D., Raymond, J., Long, K. S., McCray, R. 1997, ApJ 491, 903

Chiang, J. 2001, ApJ 549, 537

dal Fiume, D. et al. 1998, A&A 329, L41

Deeter, J. E., Boynton, P. E., Miyamoto, S., Kitamoto, S., Nagase, F., Kawai, N. 1991, ApJ 383, 324

Gerend, D. & Boynton, P. E. 1976, ApJ 209, 562

Giacconi, R., Gursky, H., Kellogg, E., Levinson, R., Schreier, E., & Tananbaum, H. 1973, ApJ 184, 227

Kahn, S. M., Leutenegger, M. A., Cottam, J., Rauw, G., Vreux, J.-M., den Boggende, A. J. F., Mewe, R., Güdel, M. 2001, A&A 365, L312

Kallman, T. R. & McCray, R. 1982, ApJS 50, 263

Klapisch, M., Schwab, J. L., Fraenkel, J. S., & Oreg, J. 1977, Opt. Soc. Am., 61, 148

Liedahl, D. A. & Paerels, F. 1996, ApJL 468, L33

Liedahl, D. A. 1999, in X-ray Spectroscopy in Astrophysics, EADN School proceedings, 1999, ed. J. A. van Paradijs, J. A. M. Bleeker, 189

Mewe, R. & Schrijver, J. 1978, A&A 65, 99

Jimenez-Garate, M. A., Raymond, J. C., Liedahl D. A. & Hailey, C. J. 2001, ApJ 558, 448

Petterson, J. A., Rothschild, R. E., & Gruber, D. E. 1991, ApJ 378, 696

Porquet, D. & Dubau, J. 2000, ApJS 143, 495

Ramsay G., Zane S., Jimenez-Garate M., den Herder J., & Hailey C., 2002, MNRAS submitted

Reynolds, A. P., Quaintrell, H., Still, M. D., Roche, P., Chakrabarty, D., & Levine, S. E. 1997, MNRAS 288, 43

Scott, D. M. & Leahy, D. A. 1999, ApJ 510, 974

Scott, D. M., Leahy, D. A., & Wilson, R. B. 2000, ApJ 539, 392

Tananbaum, H., Gursky, H., Kellogg, E. M., Levinson, R., Schreier, E., & Giacconi, R. 1972, ApJL 174, L143

Truemper, J., Pietsch, W., Reppin, C., Voges, W., Staubert, R., & Kendziorra, E. 1978, ApJL 219, L105

Wilms, J., Allen, A., & McCray, R. 2000, ApJ 542, 914